A Summary of High Peak Power (HPP) RF Processing Studies of 3 GHz Niobium Accelerator Cavities*

J. Graber†, C. Crawford‡, J. Kirchgessner, H. Padamsee, D. Rubin, and P. Schmüser†
F.R. Newman Laboratory of Nuclear Studies
Cornell University
Ithaca, NY 14853 USA

Abstract

A final summary of the High Peak Power (HPP) RF processing program with 3 GHz niobium accelerator cavities is presented. HPP has been shown unambiguously to reduce the field emission (FE) loading of the niobium cavities. Experiments have been performed on single-cell, nine-cell, and two-cell cavities. In eight tests of nine-cell cavities, average achieved accelerating gradient was improved from E_{acc} = 12 MV/m prior to HPP processing to E_{acc} = 17 MV/m following HPP processing. Through HPP processing, a two-cell cavity has sustained a continuous wave (CW) accelerating gradient of 34.6 MV/m, with corresponding peak surface electric field of 100 MV/m, record performances in each category for a superconducting accelerator cavity.

Durability of processing gains has been tested by exposing processed cavities to filtered air, at room temperature, and unfiltered air, under both room temperature and cryogenic conditions. Filtered air had no discernible effect on cavity performance. Unfiltered air degraded cavity performance, through increased emission. However much of the cavity performance could be regained through further RF processing.

We have examined the RF surfaces of several single-cell 3 GHz cavities following RF processing, in a Scanning Electron Microscope (SEM). The RF processing sessions included both High Peak Power ($P_{inc} \leq 50$ kW) pulsed processing, and low power ($P_{inc} \leq 20$ W) continuous wave processing. The experimental apparatus also included a thermometer array on the cavity outer wall, allowing temperature maps to characterize the emission before and after RF processing gains. Many sites have been located in cavities which showed improvements in cavity behavior due to RF processing. Several SEM-located sites can be correlated with changes in thermometer signals, indicating a direct relationship between the surface site and emission reduction due to RF processing.

Gains in cavity performance can be directly correlated with the magnitude of the field reached during pulsed HPP processing. RF processing of Superconducting accelerating cavities is achieved through a change in the electron field emission (FE) characteristics of the RF surface. Information gained from the SEM investigations and thermometry can be used to support the proposed model of RF processing.

Analysis of previous results of the HPP experimental program indicated that maximum fields under both pulsed and CW conditions were often limited by thermal breakdown, which is related to the surface magnetic field in the cavity. A simple thermal model accurately simulates the pulsed breakdown.

I. INTRODUCTION

Superconducting Radio-frequency (SRF) cavities are a promising technology for construction of the next generation of electron-positron colliders. In order for SRF to become a viable method for construction of these machines, however, attainable accelerating gradients must be increased from the 5-10 MV/m attained in present SRF accelerators to 25-30 MV/m.[1] Field emission (FE) of electrons from the RF surface is the primary limitation to SRF cavities. The

* Supported by the NSF with supplementary support from the U.S.-Japan Collaboration.

† Permanent Address: DESY-Tesla Group, Notkestraße 85, 22603 Hamburg, Germany.

‡ Permanent Address: Fermilab, Batavia, IL USA.

gradients reached in this work show that it is possible to achieve the desired performance for TeV colliders, using HPP to overcome field emission.

The HPP experiment was designed to explore the benefits of high power pulsed radio-frequency (RF) processing as a means of reducing FE loading in 3 GHz niobium accelerator cavities. RF processing is a method of cavity conditioning, in which the cavity is exposed to high RF fields in the absence of a particle beam. The HPP apparatus can deliver up to 170 kW peak power for millisecond pulse lengths during processing. The experimental test stand has a variable input coupling which allows the Q_{ext} to vary between 10^{10} (necessary for low power RF characterization of the cavities) and 10^5 (necessary for HPP processing), without breaking the cavity vacuum. Results of this program and descriptions of the apparatus and procedures have been presented at previous Workshops on RF Superconductivity.[2],[3] An extensive description of the entire HPP program can be found in the recently completed Ph.D. dissertation associated with this work.[4]

II. Overview of Experimental Results

A. Single-cell Cavities

Early results with HPP showed significant reduction in FE loading in single-cell cavities. These results have been presented in previous workshops, and will therefore not be repeated here. It is worth noting, however, that recently, new experiments have been performed with single cell cavities investigating the maximum attainable magnetic field on a niobium surface. The results of these experiments are being presented in another poster paper at this conference.

B. Nine-cell Cavities

Given the HPP induced reduction in FE loading in single-cell cavities, it is also important to verify that the HPP technique can successfully reduce FE loading in multi-cell structures as well as it does in single cavities. Two nine-cell cavities were constructed and tested several times each. Between successive tests on a cavity, an acid etch was performed, removing approximately 10 microns from the RF surface. Past studies lead us to believe that retesting following etching is equivalent to testing a new cavity.

Here we show that HPP is successful in improvement of low power, continuous wave (CW) behavior of the nine-cell cavities. To support this conclusion, we report on investigation of cavity performance before and after HPP processing. In section IV, we will discuss correlation of the improvements with the characteristics of HPP processing.

Figure 1 shows a histogram comparisons of attainable CW accelerating gradient and X-ray detection threshold, before and after HPP processing. X-rays are produced when emitted electrons

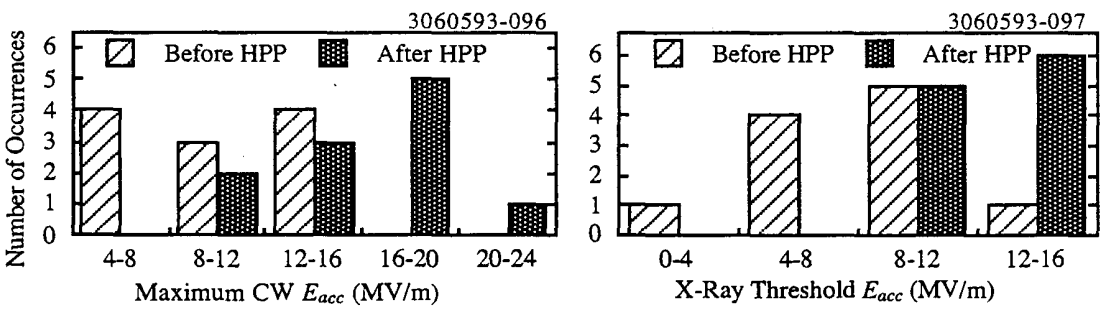

Figure 1. Histogram plots of maximum achieved CW accelerating gradient and X-ray detection threshold accelerating gradient, before and after HPP processing. For the maximum attainable gradient plot: prior to HPP, $\langle E_{acc} \rangle$ = 11.9 MV/m (s.d. = 3.4 MV/m); following HPP, $\langle E_{acc} \rangle$ = 17.0 MV/m (s.d. = 2.1 MV/m). For the X-ray threshold plot: prior to HPP, $\langle E_{acc} \rangle$ = 7.5 MV/m (s.d. = 1.3 MV/m); following HPP, $\langle E_{acc} \rangle$ = 12.4 MV/m (s.d. = 1.3 MV/m).

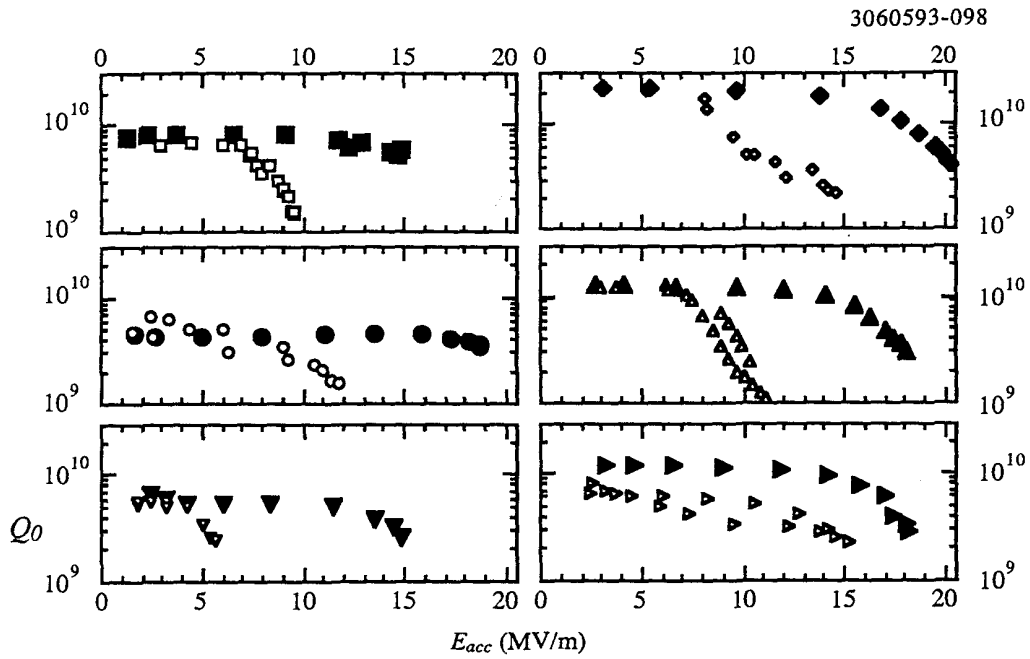

Figure 2. Composite Q_0 vs. E_{acc} plots of the six best tests of nine cell cavities. Open symbols show cavity behavior before processing; closed symbols are for after HPP.

impact elsewhere on the cavity surface. The onset of X-rays is a reproducible method of detecting the onset of FE. Generally, there is little degradation in cavity Q at the X-ray threshold. Through HPP processing, the mean attainable gradient improved from 12 MV/m to 17 MV/m, an increase of 41%. HPP processing improved the X-ray threshold gradient from 7.5 MV/m to 12.4 MV/m, an increase of 65%.

Figure 2 shows a composite plot of the Q_0 vs. E_{acc} plots of the best six experiments with nine-cell cavities. When the FE threshold is exceeded in a cavity, the dissipated power grows exponentially with increasing electric fields, causing the severe drop in Q_0, as shown in Figure 2. HPP clearly extends the usable fields of the nine-cell cavities.

C. Two-cell Cavity W3C2-1: Investigation of Reduced H_{peak}/E_{peak}

(1) Motivation

As indicated above, the initial studies were performed with single-cell and nine-cell cavities, using a geometry termed the S3C geometry. We will show below that success in FE reduction via processing is directly linked to the magnitude of the electric field attained during processing (E_{HPP}). Furthermore, it has been determined that the attainable E_{HPP} is often limited by thermal breakdown, the phenomena where the RF surface is locally heated above the critical temperature, initiating the growth of a normal conducting region. In the early HPP experiments, thermal breakdown limited single-cell cavities to E_{peak} = 55 MV/m (H_{peak} = 1265 Oe) CW and E_{peak} = 72 MV/m (H_{peak} = 1650 Oe) during HPP. Nine-cell cavities reached E_{peak} = 42 MV/m (H_{peak} = 840 Oe) CW and E_{peak} = 62 MV/m (H_{peak} = 1250 Oe) during HPP.

The S3C cavities used for the single-cell and nine-cell experiments have H_{peak}/E_{peak} ratios of 23 Oe/(MV/m) and 20 Oe/(MV/m), respectively.

(2) Cavity Fabrication and Preparation

After some investigation of potential cavity shapes, we chose a two-cell cavity using the geometry of the SRF group at the University of Wuppertal. A larger rounding of the equator region reduces the magnetic to electric field ratio of this cavity, designated W3C2-1, to H_{peak}/E_{peak}

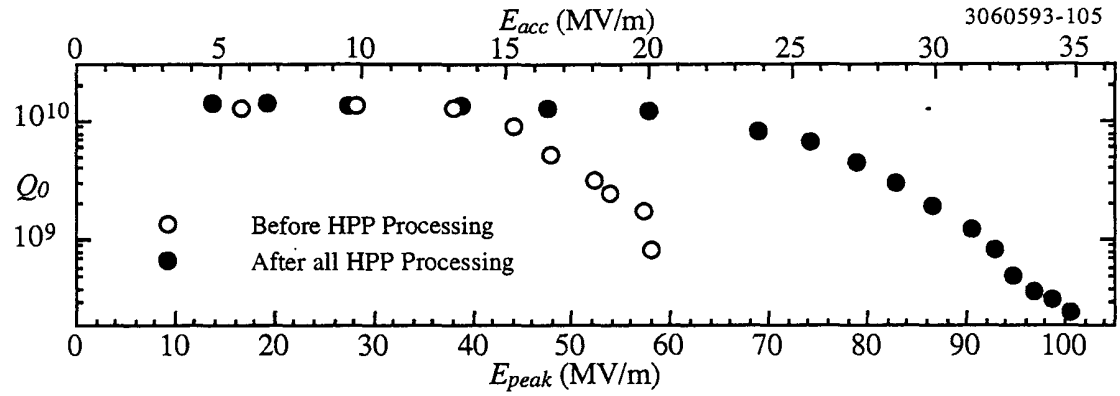

Figure 3. Q_0 vs. E_{peak} (E_{acc}) plots for the best experiment with cavity W3C2-1.

= 14.2 Oe/(MV/m). Interatom GmbH graciously agreed to press the half cells for this cavity (gratis). Final trimming, yttrification (for purification, and thus higher thermal conductivity), and electron beam welding were performed at Cornell.

The initial attempts at testing this cavity were limited by anomolously low thermal breakdown, initially due to insufficient surface chemistry then later due to excess hydrogen taken up during chemistry. The final preparation prior to the successful test was a 2 hour vacuum bake at 900° C to eliminate the hydrogen contamination.

(3) Cold RF Measurement

Based on the reduced H_{peak}/E_{peak} ratio and the observed magnetic field break-down levels (H_{bd} = 1250-1300 Oe) from the S3C cavities, we predicted that the cavity would reach 90 to 95 MV/m prior to thermal breakdown. The cavity performance exceeded this prediction. The results of the best experiment with cavity W3C2-1 are shown in Figure 3. This experiment extended over two cool downs, with a room temperature cycle, but no vacuum break between.

On initial rise of power, the cavity performance was similar to that of pre-HPP single cell cavities. FE related Q_0 drop was measurable at E_{peak} = 25 MV/m, though low power processing with P_{inc} = 10 W increased the threshold to E_{peak} = 35 MV/m. The second plot in Figure 3 is the best CW measurement from the second day of testing the cavity. This CW measurement followed processing with incident power up to 130 kW, and fields as high as E_{HPP} = 103 MV/m, a room temperature cycling, and processing with power up to 100 kW, and fields as high as E_{HPP} = 113 MV/m. During HPP, analysis indicates that Q_0 values dropped to 10^6. As can be seen, the improvement is remarkable. The maximum attained CW field was E_{peak} = 100.6 MV/m, limited by thermal breakdown (H_{peak} = 1430 Oe). This peak electric field is 20 MV/m higher than any accelerating cavity has ever been operated CW. The corresponding accelerating gradient at E_{peak} = 100.6 MV/m was E_{acc} = 34.8 MV/m. The Q_0 of the cavity remained above 5 x 10^9 for peak fields as high as 75 MV/m (E_{acc} = 26 MV/m). The experiment was repeated after another surface chemistry, reaching E_{peak} = 85 MV/m (with nearly identical field emission behavior), where it was limited by a superfluid helium leak.

D. Other Experimental Results

HPP processing is foreseen as a possible method of cavity preparation for large scale accelerator facilities. In order to show the applicability to this function, it is necessary to learn what care is required for a cavity following processing to maintain the HPP induced benefits. To this end, we first processed a nine-cell cavity (low field Q_0 = 1 x 10^{10}, $Q_0 > 10^{10}$ for E_{acc} = 14 MV/m, maximum E_{acc} = 18 MV/m) and then cycled it to room temperature. While at room temperature, the cavity was exposed to filtered air (0.3 micron HEPA filter) for 24 hours, and then re-evacuated. The cavity was then re-cooled to liquid helium temperature, and the FE behavior was measured.

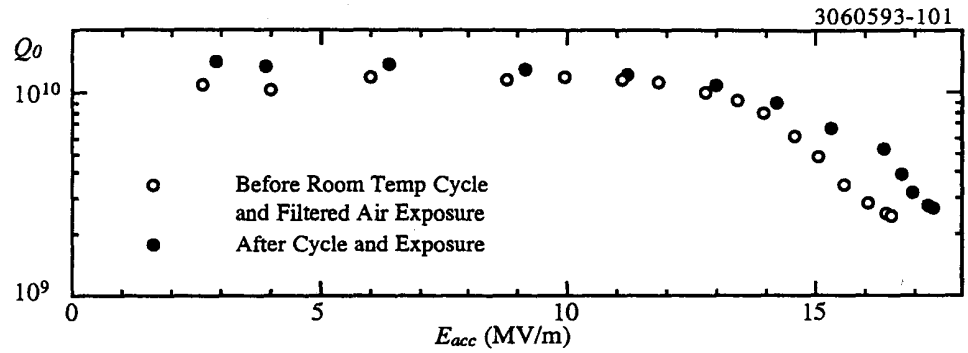

Figure 4. Q_0 vs. E_{acc} plots showing nine-cell cavity behavior before and after a room temperature cycle, with exposure to filtered air.

Figure 4 shows the Q_0 vs. E_{acc} plots before and after this exposure. No significant change in FE loading is seen. The slightly improved behavior can conceivably be attributed to removal of condensed gases from the RF surface.

The experience that exposure to clean air does not increase FE is consistent with the findings of RF processing studies performed on low frequency, heavy ion accelerator cavities at Argonne National Laboratory[5], as well as low power processing of 1.5 GHz cavities at Cornell LNS.[6]

E. Recovery from Vacuum Accidents

Vacuum accidents are an ever present danger in accelerator systems, and the contamination due to such an accident can cause significant degradation of the performance of an accelerator cavity. In this light, we present the results of two exposures of nine cell cavities to unfiltered air, one accidental and one intentional.[7] It has been established previously that air, especially unfiltered air, is a source of field emitters.[6],[8]

The circumstances of the first accident were: At $T = 4.2$ K, the cavity was exposed to the vacuum pumps which are used to evacuate the experimental dewar in order to reduce the temperature to 1.4 K. The Q_0 of the cavity fell from 2 x 10^{10} to 7 x 10^9 after the vacuum accident. Following re-evacuation of the cavity, the experiment was continued. The Q_0 vs. E_{acc} plots are shown in Figure 5. The initial rise of power was characterized by very heavy FE, some of which was processable with low power. The second curve in Figure 5 is the reproducible Q_0 vs. E_{acc}, following all possible low power processing. The cavity was then HPP processed with power as high as 90 kW, and fields as high as $E_{peak} = 58$ MV/m. The HPP processing was not only successful in reducing the FE loading, but it also improved the low field Q_0 value, possibly through RF removal of resistive contaminants on the cavity surface. The vacuum showed several

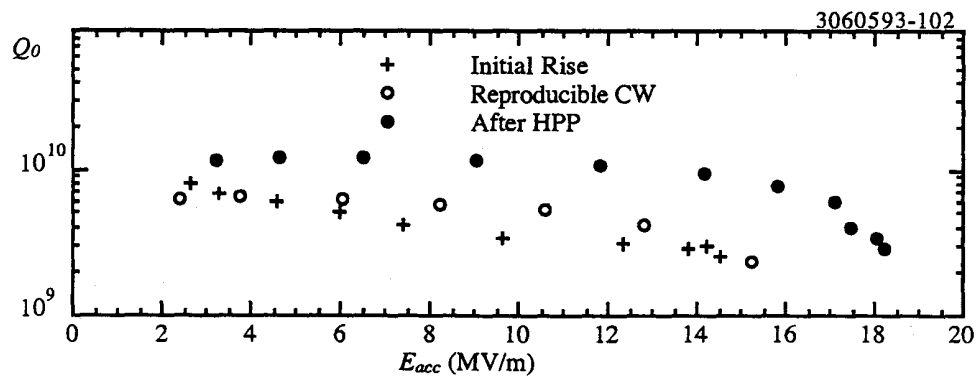

Figure 5. Q_0 vs. E_{acc} plots showing nine-cell cavity behavior before from the first vacuum accident.

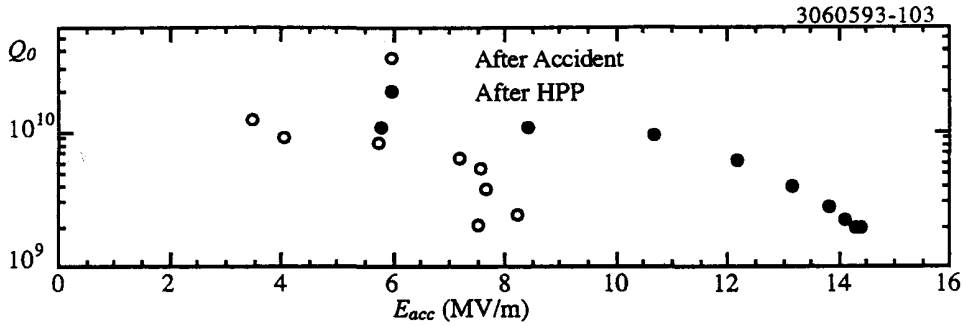

Figure 6. Q_0 vs. E_{acc} plots showing nine-cell cavity behavior before from the second vacuum accident.

fluctuations during HPP.

The second event to be reported was an intentional test of a vacuum accident. Following the above described test, the cavity was cycled to room temperature, re-cooled, and re-tested. Then, while the cavity was at liquid helium temperature, the cavity interior was exposed to unfiltered atmosphere. Following a room temperature cycle, the cavity was remeasured, showing heavy field emission, as well as a low field Q_0 degradation. The cavity was HPP processed, with peak power up to 105 kW, and fields up to E_{peak} = 42 MV/m. Again, partial recovery was made via HPP processing. The Q_0 vs. E_{acc} curves for this experiment are shown in Figure 6.

Based on these results, we conclude that if cavities are damaged by vacuum accidents, the performance may be regained through HPP RF processing, and sometimes with low power.

II. Overview of Diagnostic and Associated Investigations

A. Motivation

We report here on the effort to characterize the microscopic effects of RF processing. Surface investigation studies of the cavities in the HPP program was initiated with the goal of finding physical evidence of processing on the RF surface. We were encouraged by the findings of the Mushroom cavity project,[9] in which a specially designed, non-accelerating cavity was examined in a Scanning Electron Microscope (SEM) following RF cold tests. Multiple phenomena (e.g. "starbursts" and molten craters) were encountered in the high electric field regions of the cavity, indicating a strong link to field emission activity.

In order to better establish the link between surface features and RF processing, the experimental apparatus included an array of 100 thermometers placed in ten boards of ten resistors, spaced at 36 degree intervals around the azimuth of the cavity. Thermometers such as these have been a common diagnostic tool in SRF work for the last ten years.

SEM investigation of the cavities involves dissection of the single cell cavities in order to facilitate investigation of the RF surface, and is the final step performed on a test cavity.

B. Physical Evidence of RF Processing

It is most desirable to gather microscopic information on field emission sites before they process. DC field emission studies[8],[10] have shown that these are micron or submicron features, for example, superficial particles. Even with guidance from thermometry, where the resolution is of the order of a few square millimeters, location of such minuscule features after dissection of a cavity presents a significant challenge. Fortunately, as this study shows, if the emission site processes, or undergoes significant change during cavity operation, then the additional features associated with the processing event make it substantially easier to locate the site.

Several sites were found which have both a significant thermometry signal, a change in signal after processing, and an associated surface feature. One example of a processing event

which assumes that the emission current is consistent with the enhanced Fowler-Nordheim (F-N) theory of emission:

$$I_{FN} = \frac{C A}{\phi} (\beta E)^2 \exp\left(\pm \frac{B \phi^{\frac{3}{2}}}{\beta E}\right) \quad (1)$$

where I_{FN} is the FE current, E is the local surface electric field, ϕ is the work function of the metal, C and B are constants and β and A are the F-N field enhancement factor and emitter area, respectively. The present best model of the enhancement allows for both geometrical and material mechanisms of field enhancement. Furthermore, while no definite physical significance can be attributed to β or A, they are still useful quantities for characterizing the nature of emitters.

We therefore wish to extract values of β and A in order to better understand RF processing and its effect on emission sites. The method of extracting these values is to vary β and A in the simulation to best match the simulated with measured temperature signals on the cavity over several different electric field values. The field distribution of the fundamental mode of a cavity is such that emitted electrons follow trajectories with no azimuthal change, therefore all heating due to an emission site will be along a single board. S is the distance from the cavity equator along the cavity surface.

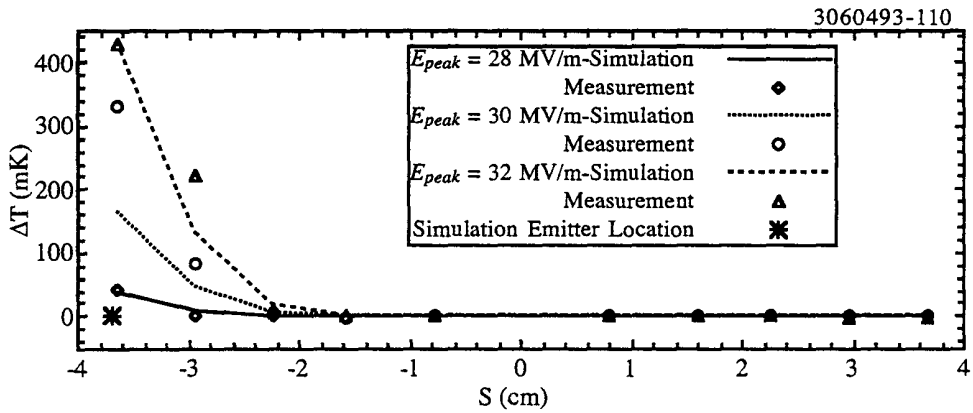

Figure 9. Comparison of measured and simulated temperature along board 8, in the first CW power rise.

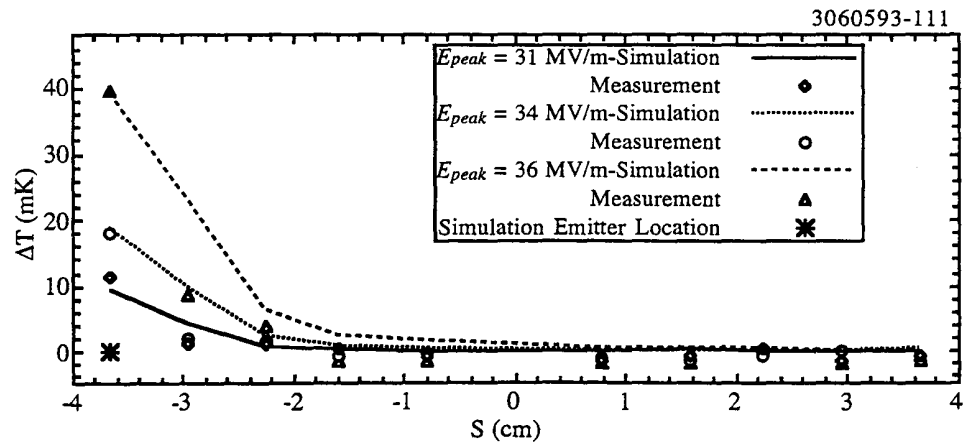

Figure 10. Comparison of measured and simulated temperature along board 8, in the final CW power rise.

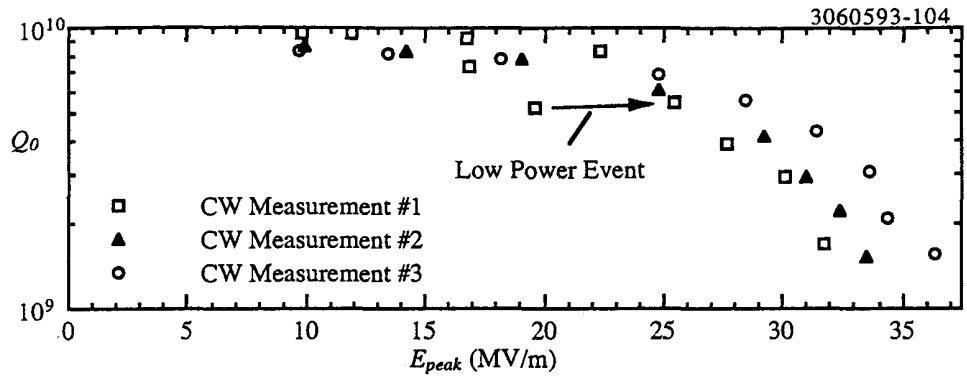

Figure 7. Q_0 vs. E_{peak} curves from low power measurements on single-cell cavity 1-5.

stands out above the rest, therefore we will expand upon this site here. This site was found in a cavity (designated 1-5) which was RF tested specifically with the goal of limiting the run to one or two processing events. More examples of SEM of niobium RF surfaces can be found in references [4] and [11].

Figure 7 shows the Q_0 vs. E_{peak} plots from the three CW power rises of this experiment. The initial CW power rise was limited by heavy FE at E_{peak} = 32 MV/m. HPP processing was then performed with P_{RF} = 2 kW, t_{RF} = 630 μsec. Peak fields during processing reached 49 MV/m. The second CW measurement was limited at 34 MV/m, again by heavy FE. The second HPP session was performed with P_{RF} = 3.5 kW, t_{RF} = 630 μsec. Peak fields during processing reached 54 MV/m. During the final CW measurement, E_{peak} reached 36 MV/m, again limited by FE.

Figure 8(a) is a temperature map of the cavity taken during the first CW measurements, at E_{peak} = 32 MV/m. The temperature map shows that the cavity was clearly dominated by a single emission site, located near the upper iris of the cavity board number 8. Figure 7 shows that, in addition to HPP processing, a processing event took place in the initial CW rise of the cavity, marked by the arrow. Inspection of the temperature maps reveal that this event was accompanied by a reduction in the heating at the dominant site shown in Figure 8(a).

Figure 8(b) is a temperature map taken during the final CW measurement, at E_{peak} = 36 MV/m. Note the reduced scale of the plot. While emission is still present, the site at the upper iris of board 8 is no longer dominating the cavity behavior. The change in heating is attributed to a change in FE characteristics through RF processing.

Given the measured change in heating, we then model the emission heating characteristics, before and after RF processing. In order to model the emission heating, we use a simulation[12]

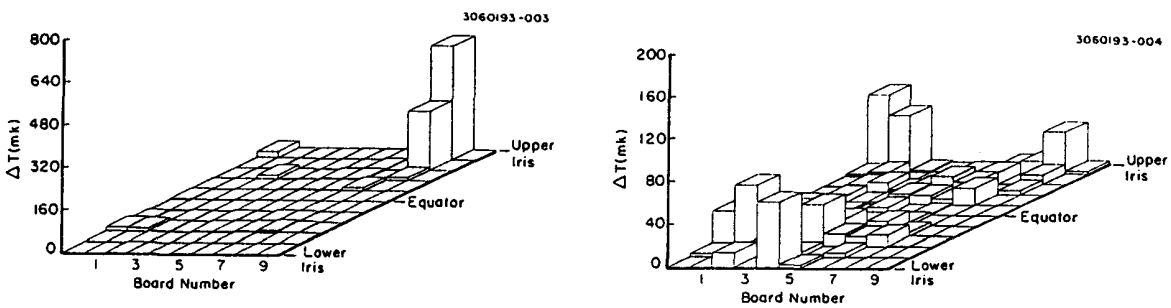

(a). E_{peak} = 31 MV/m; 1st CW power rise. (b). E_{peak} = 36 MV/m; final CW power rise

Figure 8. Temperature maps from the test of cavity 1-5.

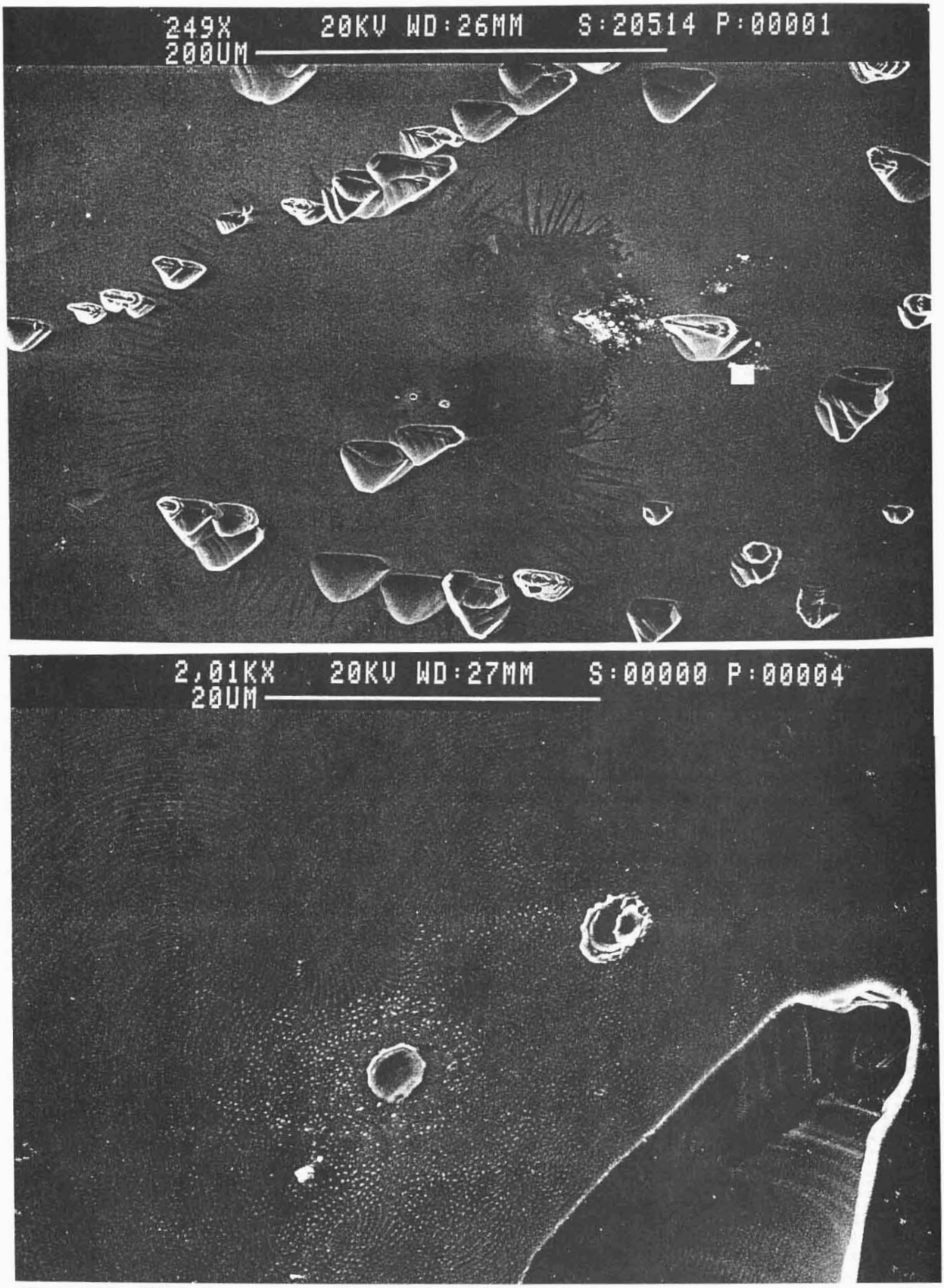

Figure 11. SEM photographs of the starburst region found in cavity 1-5. The starburst and craters are located in a position to explain the processing event. The lower picture is an enlargement of the central region of the top picture Contaminant materials include Ca, Ti, C, and O.

TABLE 1: CONTAMINANT ELEMENTS FOUND IN STARBURSTS IN HPP CAVITIES

Element	Starbursts	Element	Starbursts
Indium	19	Calcium	1
Iron	11	Silicon	1
Copper	4	Oxygen	1
Chromium	2	Carbon	1
Titanium	2		

Figures 9 and 10 show the measured and simulated temperature signals along board 8 for the initial and final CW measurements on cavity 1-5, respectively. Simulation of the initial CW rise assumes the emission source at S = -3.7, $\beta = 200$, and $A = 3.2 \times 10^{-9}$ cm^2. The simulation of the final CW power rise assumes S = -3.7, $\beta = 300$, and $A = 1 \times 10^{-13}$ cm^2.

Given this agreement between measured and simulated thermometry, the cavity was dissected and put into the SEM, for examination in the region indicated as the processed emission site. The examination was successful, as only one "starburst" feature was detected near the predicted location. Photographs of this starburst are shown in Figure 11.

As with most starbursts, the feature is dominated by a darkened (as viewed in the SEM) burst region, with diameter approximately 200 microns. At the center of this starburst are several small (10 microns) crater regions, which appear to have become molten. The craters are shown in Figure 11.

Examination of X-ray information in the SEM indicate that contaminant materials at this site include Calcium, Carbon, Oxygen, and Titanium. The crystalline appearing features are called "etch pits," and are a pitting phenomena which occur frequently in cavities which are acid etched following high temperature baking. These pits appear throughout the cavity, and therefore are not thought to be significant to the field emission aspects under study.

In all, we have examined 6 cavities following HPP processing. The general rule we have found is that the higher the fields that the cavity is exposed to, the more starbursts are found. This phenomena is demonstrated more conclusively, by examining the radial distribution of starbursts in the cavities. Figure 12 shows such a distribution, superimposed with the relative electric field along the cavity surface and aligned with a quarter cavity profile. The starbursts are well concentrated in the high field region of the cavity. This will be discussed below, when we discuss the working model of RF processing. Table 1 presents a listing of the various contaminant materials detected in starburst in single-cell cavities.

III. ANALYSIS

A. Correlation of Processing Success with Maximum Field During HPP

Given the success in improving CW behavior of the nine-cell cavities, we would like to characterize the success with relation to the terms of the HPP parameters. A clear correlation can be shown between the electric field reached during HPP processing (E_{HPP}) and the subsequent CW cavity performance. Figure 13 is a plot of maximum attained field as a function of E_{HPP}. Figure 14 is a plot of X-ray threshold as a function of E_{HPP}. In these plots we see that increasing E_{HPP} generally leads to reduced FE, and therefore increased attainable accelerating gradients. The results of the two cell cavity are in good agreement with an extrapolation of the single-cell and nine-cell results. During HPP, the input power, loaded Q, and pulse length are adjusted to maximize E_{HPP}. We additionally found that in any individual experiment, when E_{HPP} stopped improving, no further reduction of FE was achieved. Q_0 values are estimated to drop as low as 10^6 during HPP.

The primary limitation on E_{HPP} has been determined to be thermal breakdown (or quench), where the RF surface of the cavity is locally heated above the critical temperature. It then becomes normal conducting. Methods of characterizing and overcoming the quench limit will be further discussed below.

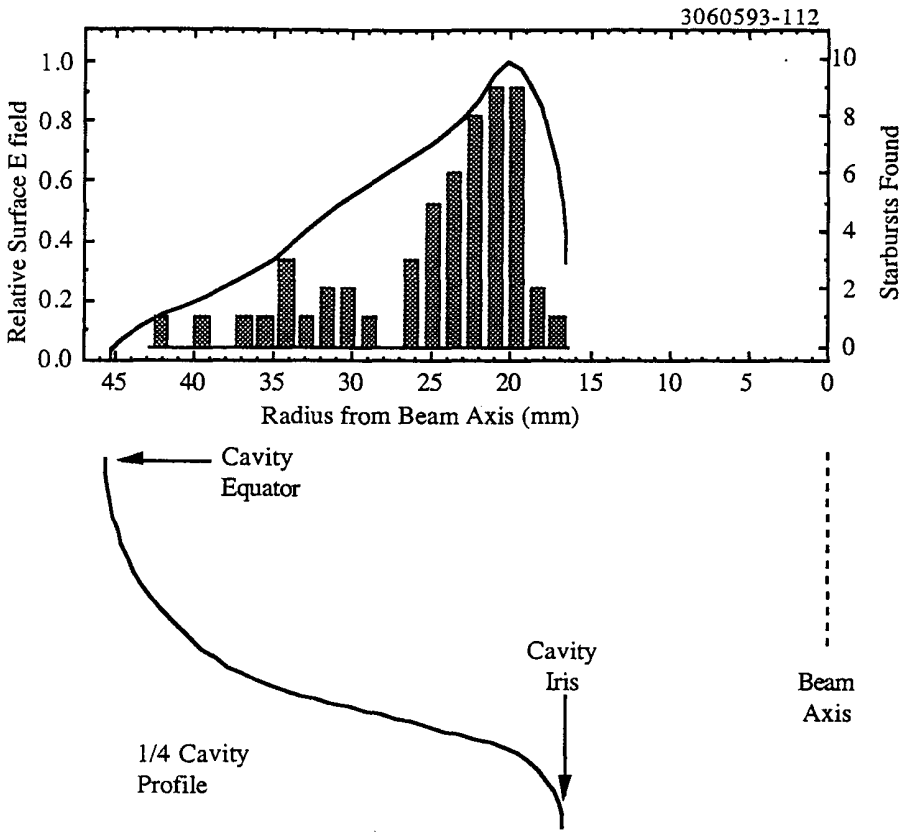

Figure 12. Radial distribution of "Starburst" phenomena found in all examined single-cell cavities, plotted along with relative surface electric field.

During application of high pulsed power, it is possible to exceed the CW thermal breakdown field while the NC region grows in size. The amount of overshoot is a function of many parameters, including incident power, CW breakdown field, loaded Q, FE loading.

The current working model for RF processing states that processing occurs when the electric fields are driven sufficiently high so as to induce an emission current which is strong enough to cause melting and/or vaporization of the emission site. This model is supported by the correlation of processing success with E_{HPP}.

Empirically, we can say that for single-cell cavities, all emission is removed to a field equal to 60% of the maximum field reached during HPP processing. Similarly, in nine-cell cavities, emission is removed for fields up to 50% of the maximum field reached during HPP processing. This empirical relationship is in good agreement with a recently developed statistical model of FE.

B. Improved Working Model for RF Processing

It is clear by the physical evidence left in the cavity following processing events that melting and/or vaporization occurs. Craters and other molten phenomena have been detected in both RF and DC emission studies, superconducting and normal conducting. The experiments reported here clearly established the link between crater/starburst sites and specific processing events. SEM investigations of HPP cavities and Mushroom cavities have shown that the Niobium, or surface contaminants, or both can become molten during processing. More than half of the starbursts examined here contained foreign elements. Other studies show that probably all the craters originated with contaminants.[13] Our EDX system was just too insensitive to detect the remaining traces following processing.

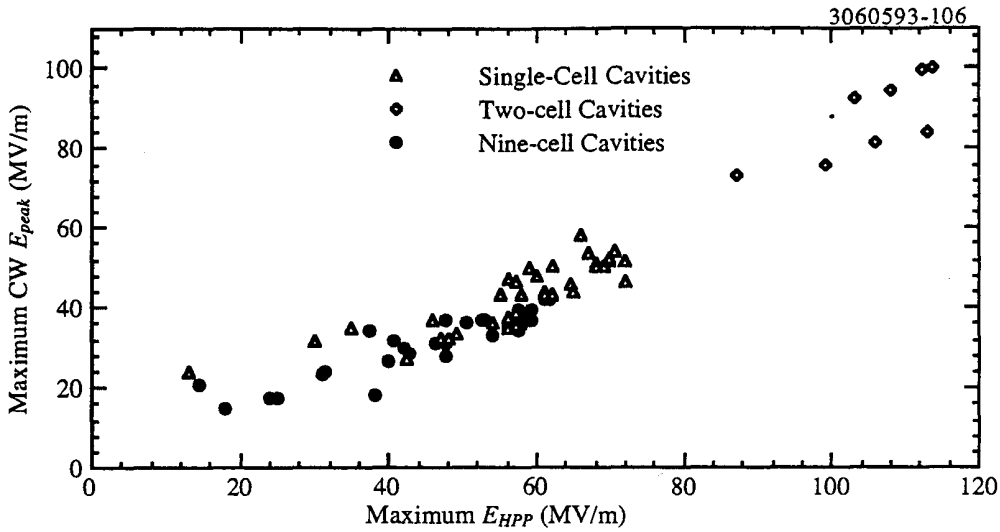

Figure 13. Maximum attained CW E_{acc} plotted as a function of maximum surface electric field during HPP processing. Note that the two-cell cavity behavior is in good agreement with an extrapolation of nine-cell and single-cell behavior.

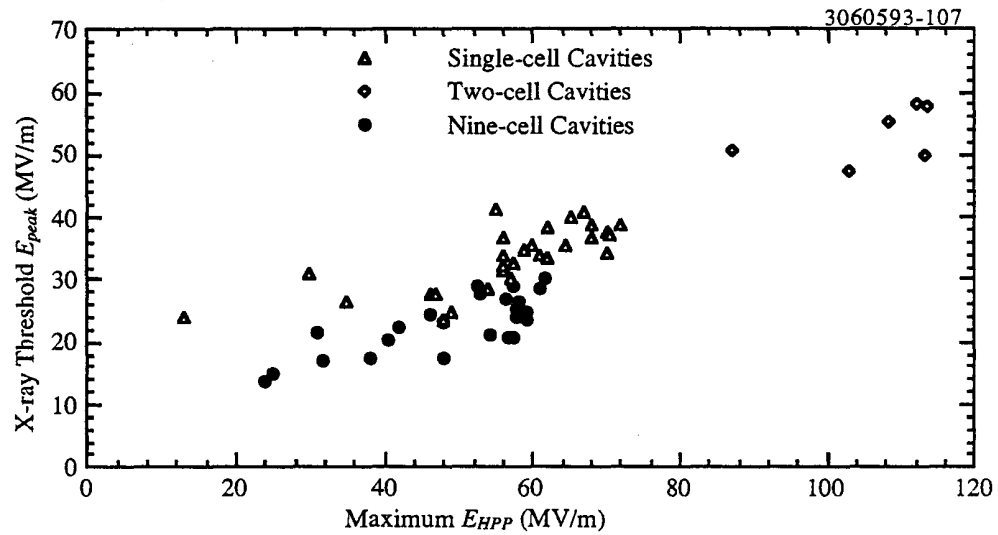

Figure 14. CW FE loading threshold E_{acc} plotted as a function of maximum surface electric field during HPP processing.

The physical nature of the craters found in these studies indicates an explosive nature of the processing event, with "splash" type features at the edges of the craters resulting from material excavation.

We examine the effect of RF processing on both the parameters β and A, as well as the current density and total current. It is important to remember that β and A are both being used to quantify emission in the F-N framework.

It is desirable to determine not only the change of F-N characteristics as a result of HPP processing, but also to determine when a site will process, based on its F-N characteristics. During HPP processing, we have no means of tracking the emission current from individual sites, and therefore no means of extracting β and A values. We can, however, obtain an estimate of processing conditions by extrapolating the current density, and total current (equation 1), by using

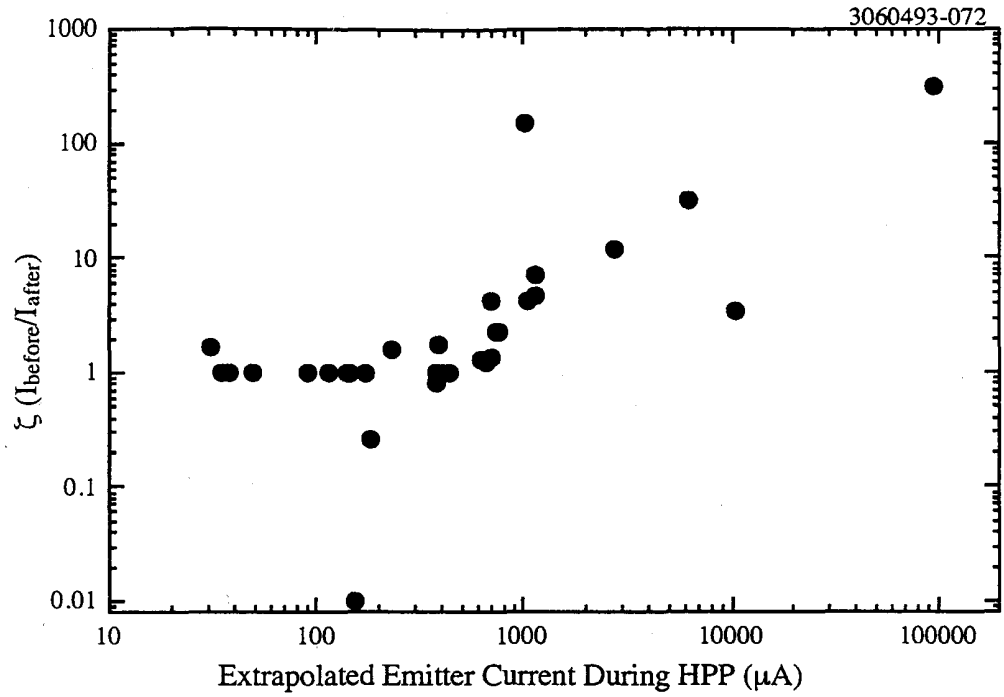

Figure 15. Emitter current reduction ratio (ζ), plotted as a function of extrapolated total current during High Power Processing.

the β and A from the CW measurements preceding the HPP processing, together with the measured fields during the HPP processing.

Success in processing is essentially reduction in total current out of an emitter. We can then define processing success in terms of a quantity ζ, the ratio of current before processing to current after processing, with both currents measured at the same CW field. The more that ζ deviates from unity, the more successful the processing. In Figure 15, we plot ζ as a function of emitter current during HPP processing. A clear pattern is apparent, showing that the larger the current which can be drawn out of an emitter, the larger the gain in performance that can be obtained. Furthermore, we see that a minimum total current of approximately 1 mA is necessary for any processing to occur. Simulations of emitters indicate that a total current of 1 mA will result in an emission related power dissipation of 100 to 1000 W (in a single-cell cavity with peak fields ranging from 50 to 70 MV/m, typical processing values), corresponding to Q_0 values of 10^8 to 10^7. Since 1 mA is a minimum current for processing success, the associated Q values are in reasonably good agreement with those obtained in the analysis of HPP behavior. No successful correlation could be made with emitter current density or β values during HPP processing.

Processing occurs when the emitter current reaches a magnitude such that the dissipated power due to Joule heating (I^2R) cannot be conducted away before melting or vaporization occurs. We conclude that the high current is necessary based on the correlation between processing success and magnitude of electric field reached. Calculations have shown that if the current density in Niobium reaches 10^9 A/cm^2, the melting temperature can be exceeded in nanoseconds.[11] Similar values of the time to reach the melting temperature have been calculated and measured in DC conditions. Such a short time is necessary in order for the material to be thermally isolated in a temporal sense. This is especially important in RF conditions, where the emitter is active for at most half of an RF cycle.

This is in good agreement with measurement and calculation in DC experiments.[11] The analysis of thermometry data from the HPP studies indicate that processing is dependent on the total current emitted.

The correlation between current and "processability" is also consistent with the overall results of HPP processing, where we have shown that success in processing is directly proportional to the maximum electric field attained during processing. The high electric fields are necessary to extract enough current out of the emitter to induce processing to occur.

It is informative to consider the advantages of HPP processing, as compared with low power CW RF processing, which make it more effective in emission reduction. The current drawn out of the emitter is strongly dependent on the electric field. The attainable electric field is in turn limited by the available power and the mechanisms which dissipate the available RF power. The rapid increase in power dissipation with increase in electric field can be overcome with a very fast rise of RF power, thus allowing for higher fields, and the correspondingly higher emission currents needed for emitter extinction. It has been clearly shown that the high emission currents make processing successful.

C. MODELING OF THERMAL LIMITATIONS

(1) The Model

With the predominance of thermal breakdown as a limitation to attainable fields during processing (and therefore success in processing), it is instructive to model the thermal processes in the cavity. Previous work on modeling (e.g. program **HEAT**[14]) has been done on the simplified system of a niobium disk, with magnetic fields (power input through dissipation) at one circular face, and a helium bath (cooling) at the opposite face. Steady state solutions of this problem provided reasonable predictions for thermal breakdown field levels in typical cavities. More recently, this model was expanded, in program **Transient_HEAT,**[15] to include transient effects. With **Transient_HEAT**, we were able to gain an initial understanding of the time evolution of a normal conducting region on a superconducting surface. With this understanding, the following model was developed.

We allow for four different loss mechanisms: superconducting wall losses, FE losses, input coupler losses, and normal conducting region losses. FE losses are estimated by extrapolating the low field FE behavior to higher electric fields.

We assume the cavity has a single breakdown initiation region, which activates at a fixed magnetic field (H_{BD}). When H_{BD} is surpassed, a circular normal conducting region begins to grow on the RF surface of the cavity, with expansion velocity v_{nc}, which was obtained by determining the growth rate of the normal conducting region as a function of magnetic field with **Transient_HEAT**. The results of **Transient_HEAT** indicate that v_{nc} varies quadratically with increasing magnetic field, with a typical growth rate being 500 m/s for $RRR = 400$, $H_{BD} = 1200$ G, $H_{surface} = 1400$ G.

A more complete description of this model can be found in the previously mentioned dissertation, as well as the paper on high magnetic fields being presented at this workshop.

(2) Model Predictions and Analysis

The result of simulation is an explanation of the relationship between the experimentally observed CW thermal breakdown field and the attainable peak field during HPP. Given the experimental conditions of RF processing, this model predicts the achievable "overshoot." Figure 16 is a comparison of measured and predicted E_{HPP}, as only the input coupling (designated by Q_{ext}) changes; pulse length and input power remain constant. The CW thermal breakdown field and the predicted peak field without taking breakdown into account are also shown for reference.

With this model, we are also able to analyze where the power is being dissipated during HPP processing. HPP was performed with 50 kW (maximum) on single-cell cavities, 130 kW on the two-cell cavity, and 200 kW on nine-cell cavities. Based on this analysis, however, we find that when thermal breakdown is occurring during the HPP, a very small part of the dissipated power is going into field emission. Figure 17 shows an example of the simulated time evolution of the

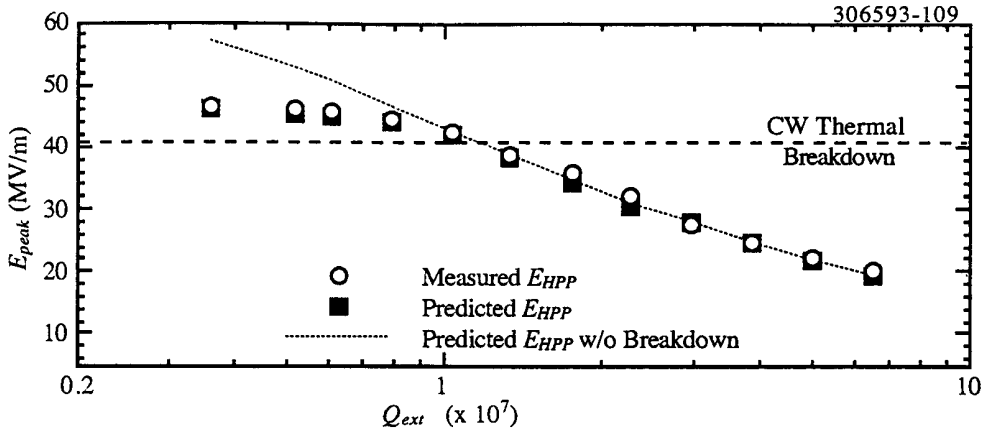

Figure 16. Comparison of Measured and Predicted E_{HPP} during HPP on a nine-cell cavity.

power dissipation in a nine-cell cavity with 200 kW peak power incident upon it. While the power dissipation reached as high as 100 kW, we find that only about 1 kW was coupled into FE. Similarly, we find that in all single-cell, two-cell, and nine-cell tests, if thermal breakdown is occurring, then FE losses account for no more than 5% of the total losses. This behavior is more clearly shown in Figure 18, where we plot the ratio of the maximum power into FE to maximum power dissipated in the cavity as a function of the maximum peak electric field reached during the RF pulse. As the CW thermal breakdown threshold is passed, this ratio plummets rapidly due to the rapidly increasing NC losses. This phenomenon makes it increasingly difficult to process the cavity to the higher fields necessary to remove the FE.

In order to optimize future HPP processing, thermal breakdown clearly must be avoided if possible. Possible methods include higher purity material, a lower RF frequency, or lower H_{peak}/E_{peak} ratios. The last method was successfully implemented in cavity W3C2-1, allowing the record performance reported here. The lower frequency approach is being implemented in the 1.3 GHz HPP program.[16]

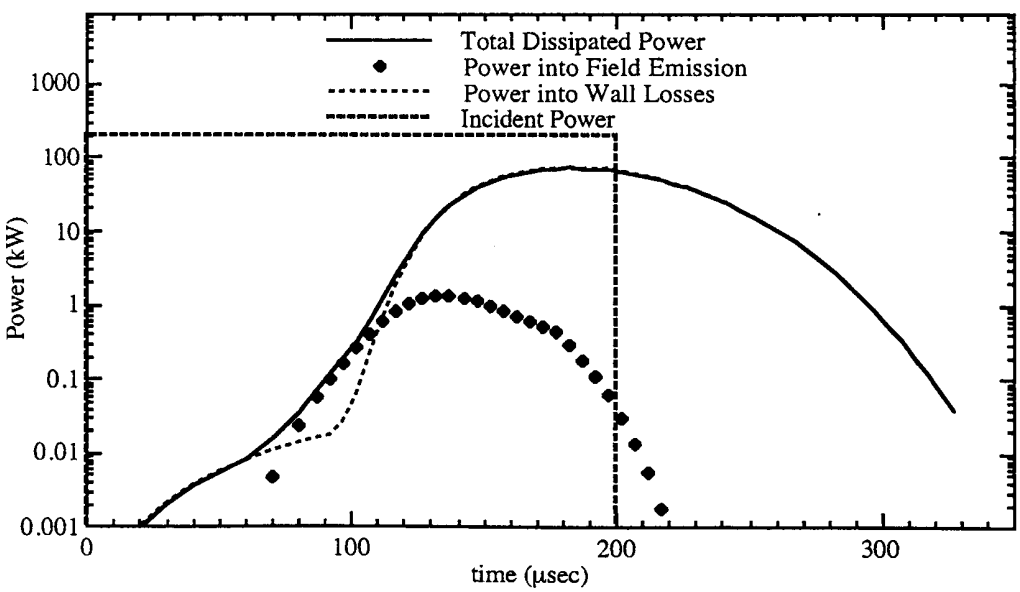

Figure 17. Power dissipation as a function of time during pulsed operation of a nine-cell cavity in quench conditions. Note that FE losses account for only 1% of total dissipation.

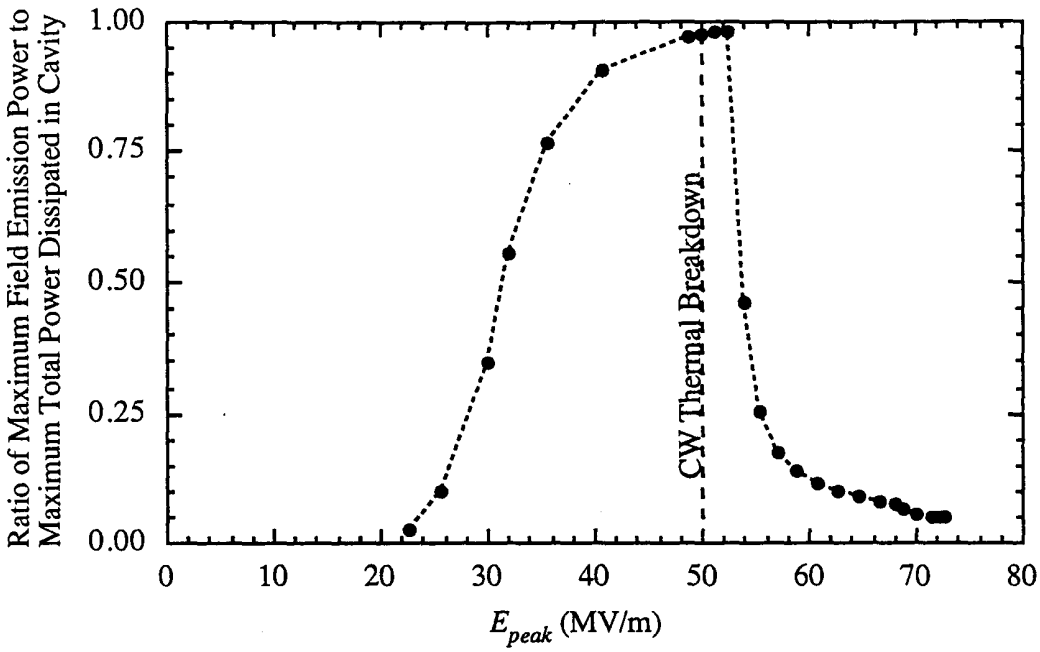

Figure 18. The ratio of maximum power coupled into field emission to the maximum power dissipated in the cavity (both simulated via the program described in the text), plotted as a function of the maximum peak electric field reached during the RF pulse. For fields less than 25 MV/m, FE is not a significant load on the cavity. As the CW thermal breakdown limit is surpassed, the expanding normal conducting region of the RF surface becomes the dominant loss mechanism.

IV. CONCLUSIONS

A. HPP as a Means of Reducing Field Emission

The HPP experiments were initiated with the primary intention of investigating high power RF processing as a means of reducing field emission loading in superconducting cavities. Based on the results described here, HPP Processing is a viable means of reducing field emission in SRF cavities. Attainable peak fields and accelerating gradients were increased up to 100% compared to before high power processing. A solid statistical data set was obtained showing the effectiveness of HPP in single-cell, two-cell, and nine-cell cavities.

Processed surfaces have been shown to be durable, in that the effects of processing are not lost when the cavity is exposed to filtered air. Furthermore, HPP processing has been shown to be an effective method of regaining cavity performance following exposure to unfiltered air (e.g. vacuum accidents), a known cause of field emission.

The strongest example of the capabilities of HPP processing was the achievement of the highest CW surface electric field ever sustained in a superconducting accelerating cavity, 100 MV/m in the two-cell cavity W3C2-1. The final accelerating gradient was 34 MV/m, also a record for an SRF cavity.

B. Determining Characteristics of RF Processing

Achieved peak field is the best predictor of the success of processing. The power level and the overall processing time are not the determining factors. Accordingly the power level, the pulse length, and the Q_{ext} of the coupler must be selected to reach the maximum E_{peak} in the face of increasing losses from FE and subsequently from a growing NC region after the onset of a thermal breakdown event.

Thermal breakdown becomes the eventual limitation to attainable fields. In spite of the thermal breakdown limit, we found that the CW thermal breakdown field could be surpassed by as much as 20 MV/m (40%), or 460 Oe under pulsed conditions with the power available to us. The extent to which cavities can exceed CW breakdown fields under pulsed conditions was explained with a simple model of a propagating normal conducting region on the superconducting surface.

C. Advances in Understanding the Mechanism of RF Processing

Correlations between thermometry and RF surface features located in the Scanning Electron Microscope indicate that the mechanism of RF processing involves an explosive emission process. Similar to DC explosive emission experiments, RF processing involves an explosive event brought on by intense field emission current. The RF processing event leaves a crater as evidence of its occurrence. The net effect of the event is reduced emission current from the emitter. Investigations also showed that the RF processing mechanism is the same in HPP processing and in rare, low power CW RF processing events.

Analysis of the thermometry data indicates that processing success is directly related to the ability to induce the emitter to produce sufficient current (approximately 1 mA) for the explosive event to occur. This is consistent with the correlation between processing success and magnitude of field reached during processing. The increasing electric field is necessary to induce higher currents from the emitters for processing.

Analysis of RF processed cavities in the SEM also solidified the link between RF surface contaminations and field emission. Contaminant materials were commonly found in the crater regions created by HPP processing events. The contaminant elements included indium, copper, iron, chromium, carbon, and titanium. Many of these contaminants can be traced to stages of cavity preparation, indicating possible gains in cavity performance with further improvement of techniques.

V. ACKNOWLEDGMENTS

The authors wish to thank Jens Knobloch and Tim Flynn for assistance with the SEM investigations of single-cell cavities, Adam Liebovitch, Karen Sauer, and Will Dickinson for assistance with the thermometry apparatus, D. Dasbach and M. Peiniger of Interatom GmbH for assistance in fabrication of the two-cell cavity W3C2-1, and Mirang Yoon and Tim Flynn for assistance with some of the calculations performed for this work.

V. REFERENCES

1 *Proc. of the 1st TESLA Workshop*, Cornell University, Ithaca, NY, CLNS **90-1029** (1990).
2 J. Graber, et al., *Proc. of the 4th Workshop on RF Superconductivity*, Y. Kojima ed., KEK, Tsukuba, Japan, **KEK Report 89-21**, 529 (1989).
3 J. Graber, et al., *Proc. of the 5th Workshop on RF Superconductivity*, D.Proch ed., DESY, Hamburg, Germany, **DESY M-92-01**, 576 (1992).
4 J. Graber, Ph.D. Dissertation, Cornell University (1993).
5 K. Shepard, Argonne Nat. Lab., priv. comm.
6 Q. S. Shu, et al., *IEEE Trans. Mag.*, **MAG-25**, 1868 (1985).
7 P. Schmüser, et al., **SRF 921117-10** (1992).
8 Ph. Niedermann, Ph.D. Thesis No. 2197, U. of Geneva (1986).
9 D. Moffat, Cornell Report **CLNS 90/991** (1990).
10 E. Mahner, this conference.
11 D. Moffat, et al., ibid. ref. 3, 245 (1992).
12 Cornell Report **CLNS/D 910121/24**, W. Hartung ed. (1989).
13 T. Hays, et al., this conference.
14 H. Padamsee, **CERN/EF/RF 82-5** (1982).

15 X. Cao, ibid. ref. 3, 727 (1992).
16 C. Crawford, et al., this conference.